Iron-mediated epigenetic activation of NRF2 targets

Horniblow, Richard D; Pathak, Prachi; Balacco, Dario L; Acharjee, Animesh; Lles, Eva; Gkoutos, Georgios; Beggs, Andrew D; Tselepis, Chris

DOI:
10.1016/j.jnutbio.2021.108929

Available online at www.sciencedirect.com

ScienceDirect

Journal of Nutritional Biochemistry 101 (2022) 108929

Journal of Nutritional Biochemistry

Iron-mediated epigenetic activation of NRF2 targets

Richard D Horniblow[a,*], Prachi Pathak[a], Dario L Balacco[b,#], Animesh Acharjee[c,d,e,#], Eva Lles[d], Georgios Gkoutos[c,d,e,f], Andrew D Beggs[d], Chris Tselepis[a]

[a] School of Biomedical Science, Institute of Clinical Science, University of Birmingham, Edgbaston, Birmingham, UK
[b] Birmingham Dental School, Institute of Clinical Science, University of Birmingham, Edgbaston, Birmingham, UK
[c] Institute of Translational Medicine, University of Birmingham, Edgbaston, Birmingham, UK
[d] Institute of Cancer and Genomic Sciences, University of Birmingham, Edgbaston, Birmingham, UK
[e] NIHR Surgical Reconstruction and Microbiology Research Centre, Birmingham, UK
[f] MRC Health Data Research UK (HDR), Midlands Site, UK

Received 9 August 2021; received in revised form 27 October 2021; accepted 7 December 2021

Abstract

The toxic effects of excess dietary iron within the colonic lumen are well documented, particularly in the context of Inflammatory Bowel Disease (IBD) and Colorectal Cancer (CRC). Proposed mechanisms that underpin iron-associated intestinal disease include: (1) the pro-inflammatory and ROS-promoting nature of iron, (2) gene-expression alterations, and (3) intestinal microbial dysbiosis. However, to date no studies have examined the effect of iron on the colonic epigenome. Here we demonstrate that chronic iron exposure of colonocytes leads to significant hypomethylation of the epigenome. Bioinformatic analysis highlights a significant epigenetic effect on NRF2 (nuclear factor erythroid 2-related factor 2) pathway targets (including NAD(P)H Quinone Dehydrogenase 1 [NQO1] and Glutathione peroxidase 2 [GPX2]); this demethylating effect was validated and subsequent gene and protein expression quantified. These epigenetic modifications were not observed upon the diminishment of cellular lipid peroxidation with endogenous glutathione and the subsequent removal of iron. Additionally, the induction of TET1 expression was found post-iron treatment, highlighting the possibility of an oxidative-stress induction of TET1 and subsequent hypomethylation of NRF2 targets. In addition, a strong time dependence on the establishment of iron-orchestrated hypomethylation was found which was concurrent with the increase in the intracellular labile iron pool (LIP) and lipid peroxidation levels. These epigenetic changes were further validated in murine intestinal mucosa in models administered a chronic iron diet, providing evidence for the likelihood of dietary-iron mediated epigenetic alterations *in vivo*. Furthermore, significant correlations were found between NQO1 and GPX2 demethylation and human intestinal tissue iron-status, thus suggesting that these iron-mediated epigenetic modifications are likely in iron-replete enterocytes. Together, these data describe a novel mechanism by which excess dietary iron is able to alter the intestinal phenotype, which could have implications in iron-mediated intestinal disease and the regulation of ferroptosis.

Keywords: Diet; Iron; Epigenome; Nutrigenetics; NRF2; Oxidative Stress; Hypomethylation.

1. Introduction

The toxic effects of free-iron within the colon are well documented, particularly in the context of inflammatory bowel disease (IBD) and colorectal cancer (CRC). It has been demonstrated that iron can contribute to disease initiation and progression through a plethora of mechanisms, including (1) ROS generation and subsequent DNA damage and/or lipid peroxidation [1–3], (2) exacerbation of the downstream effects of genetic mutations (such as APC or BRAF) [4–7], and (3) negative alterations to the intestinal microbiome [8,9]. In healthy individuals, dietary iron is absorbed within the small bowel, yet, when dietary intake exceeds the nutritional demand, which is the case in the general Western diet [10], the excess unabsorbed iron transits into the colon where it can have these detrimental effects [11]. This is particularly concerning for patients with IBD who are commonly administered oral iron supplements to remedy anemia. In such patients, this excess luminal colonic iron can further exacerbate the inflammation and have negative effects on the already dysbiotic microbiome. On the contrary, removal of iron via iron chelation can reverse these detrimental effects [12,13]. In addition to inorganic iron, the role of haem iron has been shown to promote colorectal carcinogenesis, and as such, the detrimental effects of red meat consumption are well documented [14]. These findings demonstrate a role for iron in intestinal disease initiation and progression, however, to date the impact of dietary iron on the intestinal epigenome is yet to be investigated, despite DNA methylation status being widely accepted as hallmarks of genomic alterations in disease [15]. Envi-

* Corresponding author at: Richard D Horniblow, School of Biomedical Sciences, Institute of Clinical Science, University of Birmingham, Birmingham, Edgbaston, B15 2TT, UK.
E-mail address: r.horniblow@bham.ac.uk (R.D. Horniblow).
Equal author contributions

https://doi.org/10.1016/j.jnutbio.2021.108929

ronmental influences on the epigenome, particularly with respect to dietary bioactives have been reported (including polyphenolic compounds, selenium, and curcumin) [16–18]; hence there is the possibility that iron could orchestrate intestinal epigenetic modifications and this could be an additional mechanism by which iron modulates disease progression.

In this study, we demonstrate that chronic-iron exposure does modify epigenetic signatures to colonocytes *in vitro* and the murine intestinal mucosa in mice fed with a high-iron diet. We further demonstrate that epigenetic changes are abundant within CG loci of NRF2 (nuclear factor erythroid 2-related factor 2) targets, representing a novel mechanism by which the cellular anti-oxidant response is triggered in response to iron-mediated oxidative stress.

2. Materials and methods

2.1. Cell culture

Caco-2 cells (originally obtained from the ATCC and cell authentication performed in October 2016) were routinely cultured in DMEM (Sigma, Gillingham UK) with FCS (Sigma, Gillingham UK) (10 % (v/v)), penicillin (50 U/mL), and streptomycin (50 μg/mL) (Thermofisher Scientific, UK). Prior to co-culture experiments, cells were seeded into T25 or T75 plates at a concentration of 1×10^5 cells/mL with 5 and 10 mL added respectively. Cells were co-cultured under the following conditions (1) iron sulphate ($FeSO_4$, 10 μM) (Sigma, Gillingham UK), (2) iron sulphate ($FeSO_4$, 10 μM) with glutathione (1 mM) (Sigma, Gillingham UK), (3) glutathione (1 mM) (Sigma, Gillingham UK) only, and (4) control. The concentration of iron within DMEM alone (control groups) was 0.25 μM. Cell populations were passaged 2–3 times per week depending on cell confluence throughout the 28 d culture period. The Caco-2 cells were not cultured post confluency and thus maintained a non-differentiated phenotype. After 28-d of culture cells were harvested for subsequent analyses. In some experiments, this culture period was extended by an additional 28 d whereby initially iron-treated populations were then cultured under control conditions thereafter; control cell populations were kept in control media for the full 56 d. All cell experiments were performed at a minimum in triplicate and specific experimental repetitions are provided within the figure legend of the experiment described.

2.2. Murine studies

All *in vivo* experiments were carried out under Home Office approved conditions and animal care and the regulation of scientific procedures met the criteria laid down by the United Kingdom Animals (Scientific Procedures) Act 1986. All *in vivo* experiments were carried out under Home Office approved conditions and animal care and the regulation of scientific procedures met the criteria laid down by the United Kingdom Animals (Scientific Procedures) Act 1986. All *in vivo* experiments were carried out under Home Office approved conditions and animal care and the regulation of scientific procedures met the criteria laid down by the United Kingdom Animals (Scientific Procedures) Act 1986. All *in vivo* experiments were carried out under Home Office approved conditions and animal care and the regulation of scientific procedures met the criteria laid down by the United Kingdom Animals (Scientific Procedures) Act 1986. All *in vivo* experiments were carried out under Home Office approved conditions and animal care and the regulation of scientific procedures met the criteria laid down by the United Kingdom Animals (Scientific Procedures) Act 1986.

All *in vivo* experiments were carried out under Home Office approved conditions and animal care and the regulation of scientific procedures met the criteria laid down by the United Kingdom Animals (Scientific Procedures) Act 1986. Animal studies were conducted by the University of Birmingham Biomedical Services Unit (performed under PELH as below PPL requirement). Wild-type C57BL/6 mice post-weaning were allocated into one of two experimental groups. From d 0 of the study, mice in these groups received either control diet containing 3 mg/kg ferrous sulphate as standard (Teklad, TD.80396) or the experimental iron-fortified diet containing 50 mg/kg ferrous sulphate (Teklad, TD.06015) which is identical to the control but contains the increased concentration of iron. Mice were administered these diets for 28 d. Mice had access to water ad libitum and over the period of the study were monitored for health and weight changes. All mice reached d 28, on which they were euthanized. Following dissection, intestines were removed and placed into ice-cold PBS. Intestinal tissues used for subsequent analysis were obtained by a mucosal scrape of both the small intestinal and large intestine. DNA was extracted (Qiagen DNeasy kit) and utilized for pyrosequencing as detailed below.

2.3. Determination of Caco-2 epigenetic profiles throughout 28-day iron co-culture

Throughout 28-d of culture in the presence or absence of iron, epigenetic profiles were examined using the Illumina HumanMethylation450 array system. Initially, DNA was extracted from the cells (Qiagen DNeasy kit) and subsequently bisulphite converted (Zymo, EZ-DNA Methylation kit) with a modified protocol suitable for use on Illumina microarrays (as detailed within the manufactures' protocol). A standard amplification, hybridization, labeling, and wash procedure was carried out by Genomics Birmingham (University of Birmingham). Microarrays were then scanned on an Illumina iScan array scanner and intensities were converted to IDAT files for subsequent analyses. Exported intensity data were analyzed using a combination of limma/Bioconductor and the ChAMP pipeline for methylation array analysis [19]. Data were imported into R 3.6.3 and were filtered to remove all probes that had failed the detection threshold (P>.05). Quality control plots were also produced and any samples failing Illumina standard QC were excluded. Probes were then normalized to adjust for Type 2 bias using BMIQ normalization, underwent SVD identification for components of variation, and batch correction using COMBAT. Top differentially methylated probes (DMP) were called using a 3-level regression and eBayes shrinkage of moderated t-statistics using limma.

2.4. Bioinformatic pathway enrichment analysis

We used PCA to investigate the variation among the samples (control *vs.* iron treated). A heatmap was generated using hierarchical clustering between the sample groups and the NRF2 target genes to investigate methylation changes. All the data sets were normalised using auto-scale (standardized). Analysis was performed using R(v3.6.3) (https://www.r-project.org/) and the metabolanalyst tool [20].

2.5. Pyrosequencing

Post 28-d of culture in the presence or absence of iron, pyrosequencing was undertaken on the Qiagen Pyromark Q48 Autoprep. Initially, DNA was extracted from the cells (Qiagen DNeasy kit) and subsequently bisulphite converted (Zymo EZ-DNA Methylation kit) using a standard protocol. bcDNA (1000 ng) was then subject to PCR at the regions of interest using primers designed specifically to bcDNA as described in Table 1 (Qiagen pyroPCR kit).

Pyrosequencing was undertaken using a standard protocol (Qiagen CpG Advanced reagents) on the Qiagen Pyromark Q48 Autoprep. Output data were analyzed using PyroMark Q48 Autoprep Software (Qiagen) and level of methylation was expressed as a percentage of methylated cytosines at all CG sites considered.

2.6. Human/murine genomic CG/ARE/NRF2 maps

To enable distance measurements between human CG sites analysed in this report, characterised or suspected antioxidant response elements (AREs) of NRF2 and known NRF2 transcription factor binding sites to be made, track annotations on the UCSC Genome Browser was utilized [21]. Initially, CG sites were identified from the source sequence and highlighted. Thereafter either characterized (and hence annotated) or suspect (based on the 5′-TGACnnnGC-3′ ARE motif) were highlighted [22–25]. Finally, NRF2 binding sites were annotated on the genomic maps utilizing the Transcription Factor ChIP-seq Clusters from ENCODE. This provided a visual representation of CG site location to these regulatory regions to enable correlation analysis of distance *vs.* methylation change to be calculated.

For the murine genomic mapping, the original human CG site was also annotated allowing distances between identified mouse CG sites that were analyzed in this report and original corresponding sites to be measured.

2.7. mRNA gene expression

Post 28 d of culture in the presence or absence of iron, qRT-PCR was undertaken in order to examine mRNA gene expression of genes identified as significantly hypomethylated on the methylation array. Cellular RNA (1600 ng) was extracted (Qiagen RNeasy Mini Kit) and converted to cDNA (SuperScript VILO cDNA kit). cDNA (45 ng) was then used in the quantitative RT-PCR with Taqman Gene Expression Assays (for NQO1, GPX2 and TET1) to detect mRNA expression; the 18s primer was used as the housekeeping gene for normalization (obtained from ThermoFisher Scientific, UK). Primer details are provided in Table 2.

PCR was carried out using ABI FAST Realtime PCR and 7500 RT PCR Systems (Applied Biosystems) using the following cycle: 50°C for 2 min, 95°C for 10 min, 40 repeats of 95°C for 15 s and 60°C for 1 min. Cycle threshold (ct) values were normalized relative to 18 s control to give dCt. Fold changes relative to control were calculated based on 2−ddCt (where ddCt is dCT of iron minus dCT of control for each pair).

2.8. Protein expression quantification

Post 28-d of culture in the presence or absence of iron, western blotting was employed in order to examine protein expression in Caco-2 cells of targets. The primary antibodies detailed in Table 3 were used for detection.

Table 1
Pyrosequencing primer utilised for quantification of CG methylation.

CG Site	Sequence to analyze	Gene
CG08836861	CACACACGGA	NQO1
CG09643186	GCGCAGAGTGAGCCCCGC	GPX2
Ms_09643186*	TTAACGGTATTGAGATCGTAGAACGATTTG GTAATGTAAG TTATGTTGAAGA	GPX2
Ms_14947787*	GAAATGGTCGGTAGGGAAGG TAAGGGGACGATATTTAGGGAATGTTTTGG	GPX2
Ms_19502457*	TTGTAGTTTCGGGTAGTTGTTTTTTAGAGT GACGTTATATTTTTAATTAGTATAGTTT	GPX2
Ms_0635059*	RCRTTTAAACTATTTAAAAAAAAAATAA	NQO1
Ms_0635059_2*	TTTACGGGTGAATTTGGGTTGTAGAATAAT	NQO1
Ms_10708675*	TTCGGGAGTAAGGGAGTGAGAGAGAATT	NQO1

Murine homologs (as indicated by *) of the CG sites were also utilized for pyrosequencing; the Ms_ number indicates the human CG site that the sequencing probe was developed against. Details on human-to-murine homology of these primers is provided in the supplementary information.

Table 2
Taqman gene expression assays utilized for mRNA expression analyses.

Gene	Taqman #	Padded amplicon sequence
NQO1	Hs01045993_g1	AAGAAAGGATGGGAGGTGGTGGAGTCGGACCTCTATGCCATGAACTTC AATCCCATCATTTCCAGAAAGGACATCACAGGTAAACTGAAGGACCC TGCGAACTTTCAGTATCCTGCCGAGTCTGTTCTGGCTTATAAAGAAGG
GPX2	Hs01591589_m1	TTGGACATCAGGAGAACTGTCAGAATGAGGAGATCCTGAACAGTCTCAA GTATGTCCGTCCTGGGGGTGGATACCAGCCCACCTTCACCCTTGTCCA AAAATGTGAGGTGAATGGGCAGAACGAGCATCCTGTCTTCGCCTACCTGAAGG ACAAGCTCCCCTACCCTTATGATGACCCATTTTCCCTCATGACCGATCCCAAGCT CATCATTTGGAGCCCTGTGCGCCGCTCAGATGTGGCCTGGAACTTTGAGAAG TTCCTCATAGGGCCGGAGGGAGAGCCCTTCCGACGCTACAGCCGCACCTT CCCAACCATCAACATTGAGCCTGACATCAAGC
TET1	Hs04189344_g1	GTGCACAGAAAAATTTTAATGATTATGCCATGAACTTCTTTACTAACCCTAC AAAAAACCTAGTGTCTATAACTAAAGATTCTGAACTGCCCACCTGCAGCTGTC TTGATCGAGTTATACAAAAAGACAAAGCCCATATTATACACACCTTGGGGC

Table 3
Antibodies utilized for Western blotting studies for protein expression analyses

Protein	Identity #	Dilution in 1X TBST with 5 % (w/v) milk	Expected MW (kDa)
NQO1	D6H3A (Cell Signaling Technology)	1:2000	29
GPX2	MAB5470 (R&D systems)	1:200	22
FTH1	ab69090 (Abcam)	1:2000	22
Beta-Actin	ab8226 (Abcam)	1:2000	44

Secondary antibodies (Jackson ImmunoResearch Europe LTD, Rabbit: AB2307391, Mouse: AB2338447) were used at a dilution of 1:10,000 in 1X TBST-Milk (5 % w/v). Expression of all proteins of interest were normalized against β-actin. All blots were subject to densitometry analysis using ImageJ analyzing software.

2.9. Lipid peroxidation & malondialdehyde (MDA) assay

Post 28-d co-culture in either (1) iron sulphate ($FeSO_4$, 10 μM), (2) iron sulphate ($FeSO_4$, 10 μM) with glutathione (1 mM), (3) glutathione (1 mM) only, or (4) control cell lysates were harvested and protein was quantified using the Pierce BCA assay (ThermoFisher Scientific, Assay# 23225). Subsequently, MDA concentrations were obtained using the (Lipid Peroxidation Assay Kit (Colorimetric/Fluorometric) (ABCAM, ab118970) according to the manufacturer's protocol. MDA concentrations were normalized to protein concentration.

2.10. Quantification of the labile iron pool (LIP)

To quantify the LIP, Calcein-AM (Corning) was utilized as a fluorescent probe according to a previously reported protocol [26]. For each sample, 10,000 events are captured within FL-1.

2.11. Quantification of intracellular iron levels (Ferrozine assay)

To quantify the concentrations of intracellular iron throughout co-culture with iron the ferrozine assay was employed using a previously published protocol [27]. Iron concentrations were normalized to protein concentration

2.12. Absolute quantification of ferritin protein concentration

Post 28 d co-culture in the presence or absence of iron sulphate ($FeSO_4$, 10 μM), cells were harvested and lysed in RIPA buffer before ferritin concentration was determined using the ORIGENE Human Ferritin ELISA kit (EA100984) according to the manufacturer's protocol. Ferritin concentrations were normalized against protein concentrations.

2.13. Correlation of tissue methylation status to gene expression

The TCGA colon adenocarcinoma (COAD) [28] DNA methylation and gene expression data were downloaded from the NCI Genomic Data Commons (GDC) Legacy Archive [29] using the Bioconductor package TCGAbiolinks (version 2.14.1) [30–32] in R (version 3.6.3) [28]. DNA methylation data were generated from Illumina Human Methylation 450k arrays; gene expression data were generated

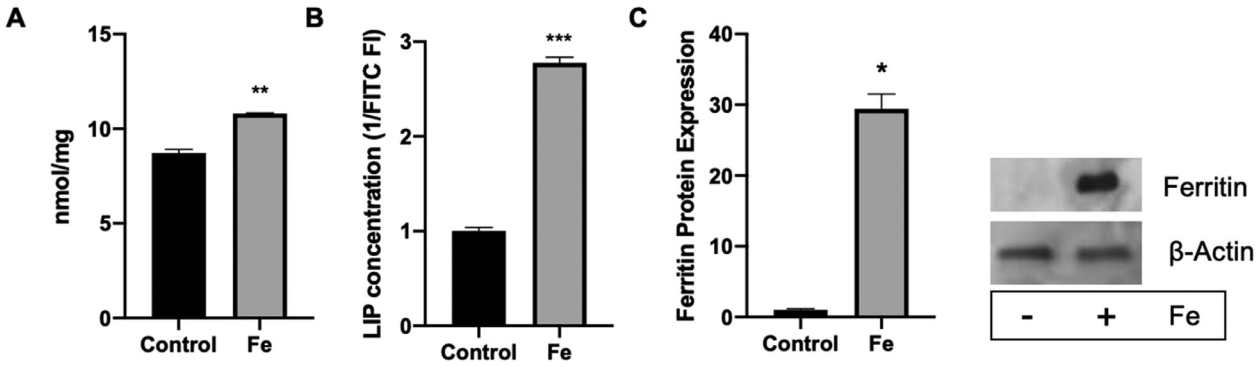

Fig. 1. Cellular iron metabolism changes. (A) Ferrozine assessment of cellular iron concentrations and (B) LIP quantification of Caco-2 after 28-d of co-culture in the absence or presence of $FeSO_4$ (10 μM). (C) Ferritin protein expression after 28-d of co-culture in the absence or presence of $FeSO_4$ (10 μM). Data displayed as mean values (n=3 for each experiment) with error bars representing +/- standard deviation. Significant changes examined using a paired students t-test where *, ** and *** denotes P<.05, 0.01 and .001 respectively.

from RNA-seq using the Illumina HiSeq platform. Solid normal tissue accessions with both DNA methylation and gene expression data annotated were selected for the analyses (see supplementary data for sample barcode tables). Data were prepared, normalized, and filtered, as described in Silva et al. 2016. Differential expression analyses were performed using the TCGAbiolinks' function TCGAanalyze_DEA (fdr.cut=0.01, logFC.cut=1, and method=glmLRT).

2.14. Statistical analyses

All data were analyzed using the Graph Pad Prism 8.4.1 statistical software. Differences between two groups were analyzed using Student's t-test. Differences between more than two groups were analyzed using repeated measures ANOVA. Two-sided *P*-values of <.05 were regarded significant unless otherwise stated within the experimental result. False Discovery Rate (FDR) adjusted *P*-values were calculated by "*P*.adjust" method in R, and FDRs <.05 were considered to be significant. Two-sided Pearson's correlation tests and correlation plots were conducted using the "cor.test" method in R.

3. Results

3.1. 28-day iron co-culture and subsequent cellular iron metabolism changes

Caco-2 cells were co-cultured with iron for 28 d and cellular iron-status was validated by cellular iron-concentration measurements (Fig. 1A), Labile Iron Pool (LIP) examination (Fig. 1B) and FTH1 protein expression changes (Fig. 1C).

Both intracellular iron levels and the LIP increased (1.2 and 2.7-fold increase compared to control respectively) in Caco-2 cells treated with iron for 28 d. Correspondingly, FTH1 protein expression increased by 29-fold in cells co-cultured with iron. This validates that long-term (28 d) exposure to low-dose (10 μM) iron results in cellular iron-loading and the expected changes in cellular iron metabolism.

3.2. Assessment of the Caco-2 epigenome post iron-exposure

With confirmation that cellular iron metabolism changes are incident under the conditions employed, Caco-2 cells treated with iron under the same conditions were harvested and bsDNA subject to genome-wide methylation status analysis using the Illumina HumanMethylation450K BeadChip platform. Methylation change data (treatment [Fe] *vs.* control [no Fe]) can be accessed within the supplementary information.

Principal component analysis (PCA) was performed utilising methylation signals from all CG sites (Fig. 2A). This analysis revealed significant differences in methylation profiles between iron and control treated populations (n=4). The total number of significant hypomethylated CG sites induced by iron was 157 (β>10); no significant hypermethylated CG sites were identified. Following a pathway enrichment analysis and identification of differentially methylated NRF2-associated CG sites, hierarchical clustering of samples based on the identified NRF2 targets (ALD3H1A, SQSTM1, GPX2, EPHA2, NQO1) was performed (Fig. 2B). A clear separation of iron-treated and control populations was observed. All NRF2 targets were hypomethylated by iron and average changes in methylation were: EPHA2 [CG03258665: 8.5 %, CG09178261 4.1 %, CG27582323 8.0 %]; SQSTM1 [CG15126957 8.4 %, CG08836954 13.8 %, CG01152073 6.3 %, CG01325271 4.8 %, CG12619504 4.9 %]; GPX2 [cg13844922 15.1 %, CG09643186 13.1 %, CG19502457 10.9 %, CG14947787 7.2 %]; NQO1 [CG08836861 14.3 %, CG19194454 5.0 %, CG26598152 6.3 %, CG06359059 2.6 %, CG10708675 4.1 %]; ALDH3A1 [CG13295878 7.1 %, CG27329371 8.5 %, CG00516966 7.8 %, CG25145360 5.8 %, CG00855466 3.8 %, CG15726326 6.2 %] and SLC39A11 [CG16434331 23.3 %] (adj. $p < 0.05$). Literature based evidence of known NRF2 targets adopted from WikiPathways (WP2884)[33] and methylation changes obtained from the array identified 56 from a 141 NRF2 gene targets, of which all were significantly hypomethylated (adj. P<.05) by iron (Table 4).

3.3. Validation of iron-dependent hypomethylation and subsequent cellular metabolism changes of NRF2 targets

Bioinformatic-led analysis identified iron-mediated hypomethylation of NRF2 targets. To validate these observations, key NRF2 targets (NQO1 and GPX2) were examined for methylation status changes post iron treatment using pyrosequencing (Fig. 3A). Additionally, the influence of CG demethylation on NQO1 and GPX2 mRNA expression (Fig. 3B) and subsequently NQO1 and GPX2 protein expression (Fig. 3C) was determined.

Examination of CG-site specific methylation status demonstrated significant hypomethylation changes; 16 and 29% for NQO and GPX2 respectively. These were similar in magnitude to the hypomethylation changes found using the 450K array. Additionally, qRT-PCR gene expression analysis of key NRF2 targets (NQO1 and GPX2) revealed increased mRNA expression in iron-treated populations; 3.8 and 9.6-fold for NQO1 and GPX2 respectively. Furthermore, increases in mRNA expression were found to be translated into protein expression where NQO1 and GPX2 were 9.4 and 2.8-fold increased in expression in iron-treated populations respectively.

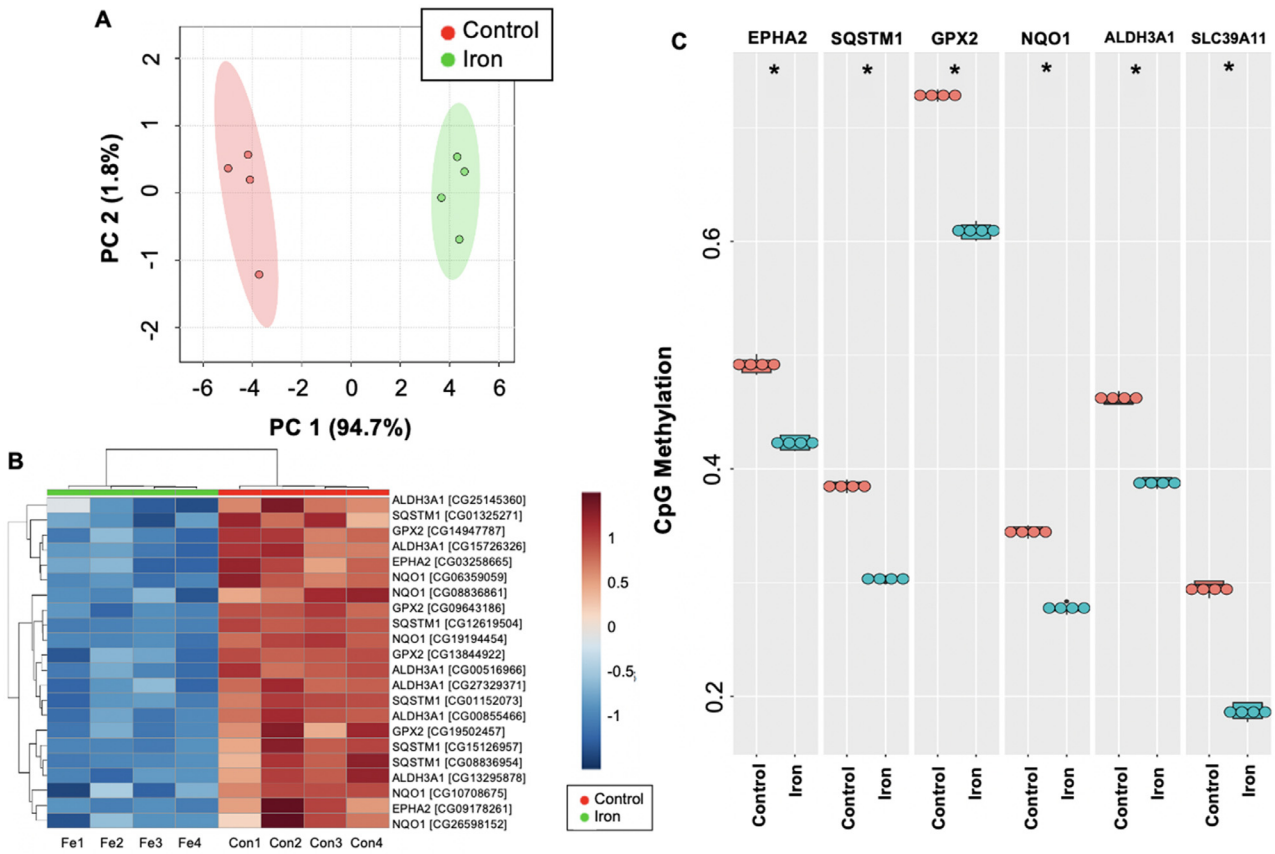

Fig. 2. Epigenome wide screen of methylation changes induced by chronic iron co-culture. (A) Principal component analysis (PCA) and score plot of DNA methylation profiles in iron treated (green, *n*=4) and control (red, *n*=4) independent Caco-2 populations. (B) Heat map with hierarchical cluster analysis of the methylation array data, based on NRF2 CG loci. (C) Box plot showing average methylation status of iron and control treated Caco-2 cells (*n*=4 for each population) for EPHA2, SQSTM1, GPX2, NQO1, ALDH3A1 and SLC39A11 NRF2 targets as assessed from the methylation array. NRF2, nuclear factor erythroid 2-related factor 2.

3.4. Iron-dependent methylation changes are time-dependent and reversible

Expression differences of the NRF-2 targets and cell iron-metabolism changes were examined over the time course of the 28 d iron co-culture period to examine how the observed changes (at d 28) were established on a week-by-week basis (Fig. 4).

At week 1 (d 7) no significant differences were observed in any of the parameters examined iron and control treated cells. At week 2 (d 14) the only change was observed in cell ferritin protein concentrations, with a 1.4-fold increase in the iron treated cells. At week 3 (d 21) significant changes were observed; MDA (a measure of cellular oxidative stress) concentrations were increased by 18-fold, intracellular iron increased by 1.2-fold, ferritin concentration increased by 11-fold, GPX2 and NQO1 protein was increased by 1.3 and 31-fold respectively, the LIP was increased 2-fold and GPX2 and NQO1 gene expression were all elevated compared to control. Similar, if not greater, increases were observed at week 4 (d 28) for all measured characteristics.

In order to examine if the methylation, gene and protein expression effects orchestrated by iron-exposure are long standing and irreversible, Caco-2 cells again were subject to 28-d chronic iron exposure and subsequently cultured in an iron-free media for an additional 28 d. Following this, methylation status, mRNA, and protein expression were quantified (Fig. 5).

Significant changes in methylation status of NQO1 and GPX2 as assessed using pyrosequencing were only measurable after 24–28 d of iron co-culture. Upon removal of iron, methylation status returned to baseline, mRNA expression returned to control levels and there was no significant difference in protein expression between iron treated and control Caco-2 populations.

3.5. Iron is inducing methylation changes via oxidative stress

To determine if oxidative stress could be orchestrating the methylation changes and inducing the cellular subsequent phenotypes as detailed, investigations quenching the oxidative nature of iron and subsequent impacts on methylation status were determined (Fig. 6).

Chronic exposure to iron induced TET1 gene expression in Caco-2 cells 2.1-fold relative to control (Fig. 6A). Measurement of malondialdehyde (MDA) as a surrogate marker for cellular lipid peroxidation of Caco-2 cells subject to 28 d iron exposure demonstrated that in iron-treated populations a significant 400-fold increase in MDA concentrations was observed (Fig. 6B). Furthermore, in cell populations that were additionally co-cultured in the presence of exogenous glutathione (GSH) alongside iron, MDA concentrations returned to near baseline levels. Similarly, when Caco-2 cells were co-cultured under these iron +/- GSH conditions, pyrosequencing of NQO1 and GPX2 CG sites revealed changes in methylation status (Fig. 6C). As expected, co-culture with iron alone resulted in hypomethylation (from 25 to 9% and from 97 to 43 % for NQO1 and GPX2 respectively). With the addition of GSH, significant increases in methylation were observed (albeit not to original control levels); NQO1 CG methylation increased by 10 % and GPX2 methylation increased by 31 %.

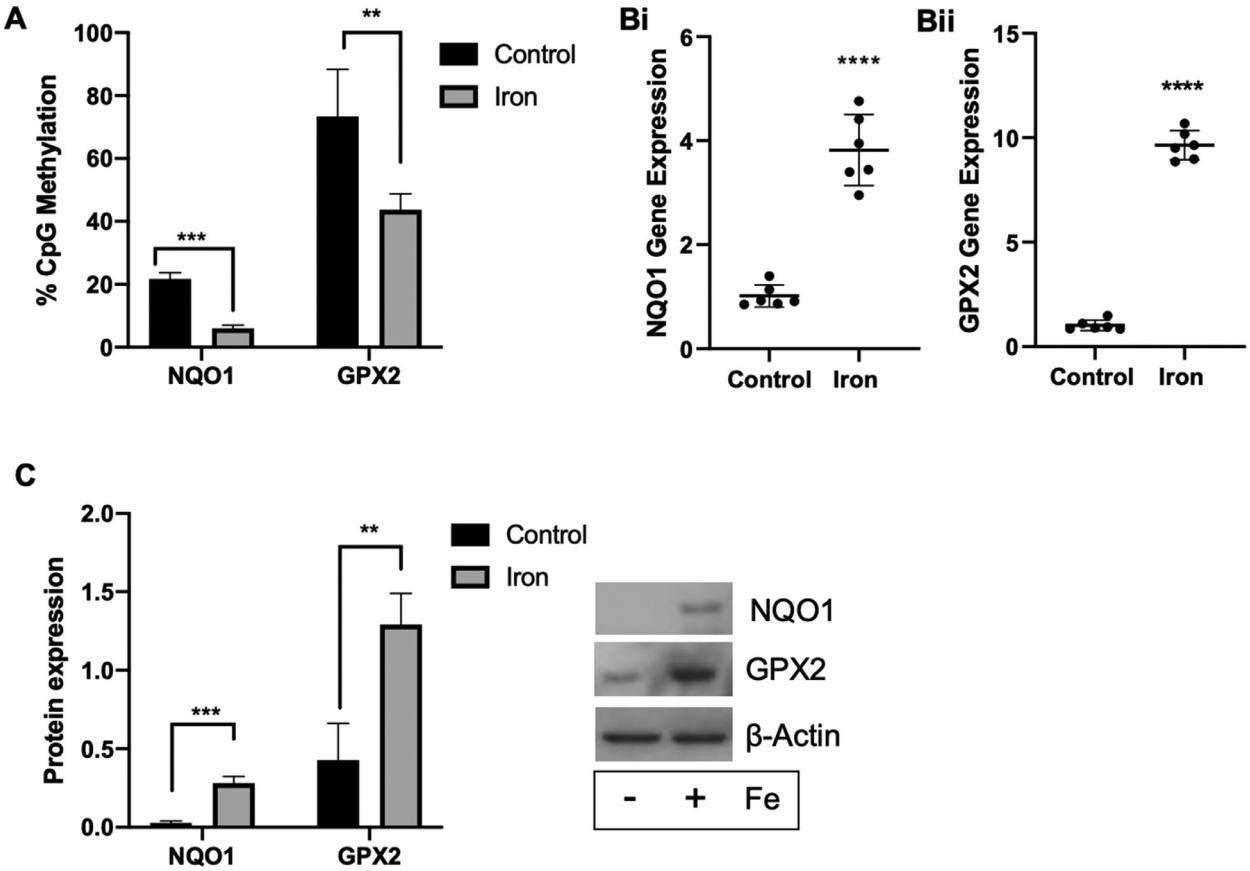

Fig. 3. Validation of iron-induced methylation changes and subsequent gene and protein expression changes. (A) Validation of methylation changes analyzed using pyrosequencing at targeted CG sites within the genes of NQO1 and GPX2 in Caco-2 cells co-cultured for 28-d with $FeSO_4$ (10 μM). (Bi) NQO1 and (Bii) GPX2 gene expression after 28-d of co-culture in the absence or presence of $FeSO_4$ (10 μM). (C) NQO1 and GPX2 protein expression after 28-d of co-culture in the absence or presence of $FeSO_4$ (10 μM). Data points represent mean values (n=3 for each experiment), with error bars representing +/- standard deviation. Significant changes examined using a paired students t-test where *, **, *** and **** denotes P<.05, .01, .001 and .0001 respectively.

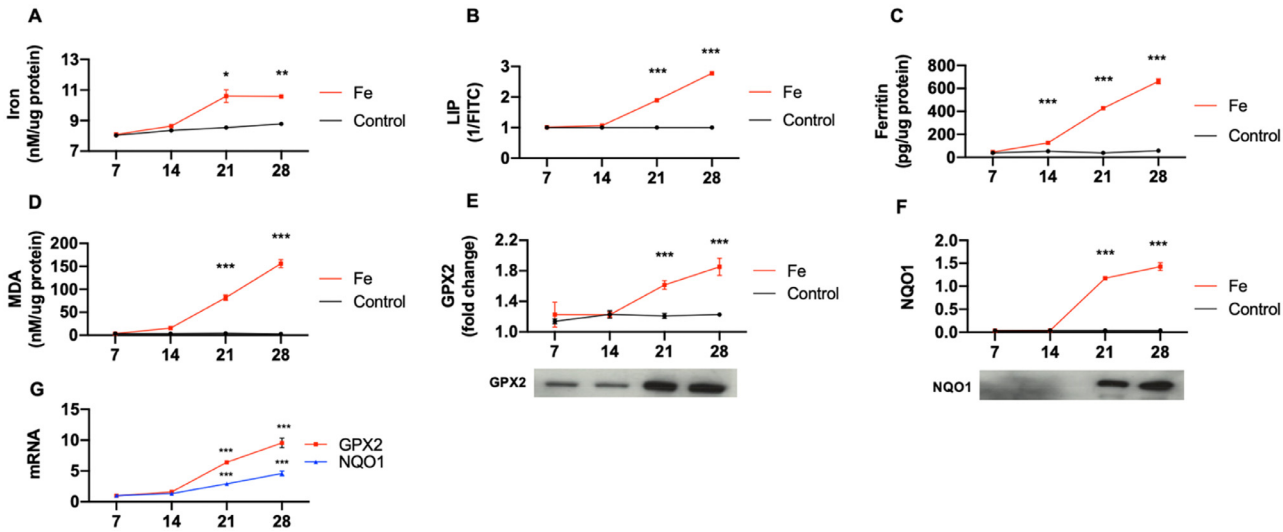

Fig. 4. NRF-2 target activation and correlations with cellular iron metabolism changes. Analysis of (A) intracellular iron concentrations, (B) LIP concentrations, (C) ferritin protein levels, (D) MDA concentrations, (E) GPX2 and (F) NQO1 protein expression changes as analysed by Western blot and (G) GPX2 and NQO1 gene expression (fold changes relative to control) every 7-d throughout the 28-d co-culture in the presence or absence of iron. Data presented as mean values (n=3 at each time point), with error bars representing +/- standard deviation. *, ** and *** denotes statistical significance where P<.05, 0.01 and .001 respectively. LIP, labile iron pool; MDA, malondialdehyde; NRF2, nuclear factor erythroid 2-related factor 2.

Table 4
All NRF2 associated CG sites identified in the methylation array. Methylation change reported is Fe relative to control.

CG site	Adj. *P* value	Beta	% Methylation change	Gene
cg16434331	2.55E-05	12.8	23.2	SLC39A11
cg00339695	0.00036	6.47	15.5	SLC5A11
cg13844922	4.61E-05	10.68	15.1	GPX2
cg08836861	3.59E-05	11.57	14.3	NQO1
cg09502149	0.00015	8.19	13.8	SLC2A1
cg25132662	0.0012	8.52	13	TGFB2
cg12763828	0.00082	5.023	12.2	SLC2A5
cg02688643	0.0013	4.14	11.7	MGST2
cg06784602	0.0007	5.29	11	TGFBR2
cg08305799	0.019	-0.03	10.6	GSR
cg22247664	0.00072	5.2	10.4	GSTM4
cg14592673	0.00022	7.44	9.7	ABCC3
cg21297772	0.0037	2.52	9.6	SLC5A9
cg07062764	0.0017	3.74	9.4	SLC2A2
cg13617376	0.00019	7.18	9.3	ABCC2
cg03258665	0.002	3.47	8.5	EPHA2
cg15126957	5.65E-05	10.24	8.4	SQSTM1
cg01106989	0.0053	1.95	8.4	GSTA4
cg12060132	0.021	-0.15	8.1	CYP4A11
cg20803780	0.036	-1.01	7.9	GSTA1
cg25117600	0.0024	3.21	7.9	SLC2A9
cg13295878	0.00021	7.53	7.1	ALDH3A1
cg05914981	0.012	0.56	7.1	AGER
cg09121478	0.0003	6.84	6.9	SLC2A7
cg09968361	0.0012	4.36	6.8	SERPINA1
cg06697339	0.0014	4.17	6.3	SLC5A5
cg27610561	0.0087	1.17	6.2	SLC2A10
cg06829969	0.035	-0.97	6.1	PGD
cg03606774	0.021	-0.19	6.1	SLC5A6
cg21382890	0.031	-0.81	5.7	NFE2L2
cg09950076	0.0041	2.37	5.5	UGT1A6
cg09136245	0.023	-0.36	5.5	SLC6A5
cg05972316	0.0085	1.22	5.3	SLC6A19
cg01921382	0.0019	3.62	5.2	SLC6A18
cg26925717	0.025	-0.45	5.2	SLC39A2
cg05412906	0.011	0.79	5	HSP90AA1
cg15859995	0.012	0.61	4.8	GSTA5
cg22123459	0.0085	1.22	4.5	GGT1
cg26538442	0.018	-0.01	4.5	CES3
cg09230938	0.0016	3.82	4.4	ABCC5
cg05718255	0.0109	0.81	4.2	HMOX1
cg24375085	0.039	-1.18	4.2	SLCA16
cg22224704	0.031	-0.8	4.1	GSTP1
cg24767336	0.014	0.42	4.1	TGFB1
cg08926287	0.0285	-0.67	4.1	SLC6A6
cg02257517	0.0081	1.3	4	SLC2A6
cg07933378	0.0067	1.6	4	SLC39A4
cg00521255	0.0254	-0.49	3.7	HBEGF
cg14348706	0.014	0.46	3.3	SLC39A7
cg13831329	0.017	0.12	3.2	PTGR1
cg21212995	0.0094	1.05	3.2	SLC6A7
cg04454259	0.022	-0.32	3.1	CBR3
cg01330016	0.0175	0.093	2.7	SLC6A4
cg09079613	0.027	-0.63	2.4	SLC39A1
cg06873218	0.03	-0.75	2.3	PDGFB
cg13363904	0.028	-0.65	-4.2	SLC5A12

3.6. Degree of NRF2 CG target hypomethylation is not correlated to distance from antioxidant response elements (AREs) or NRF2 transcription factor binding sites (TFBS)

Iron would induce the transcription of NRF2 targets via transcription factor binding; KEAP1 [Kelch-like ECH-associating protein] would become oxidised resulting in NRF2 stabilization, nuclear translocation and transcriptional activation by binding to AREs (referred to as Canonical activation hereafter). Consequently, NRF2/ARE binding could block DNA methylation by, for example, DNA (cytosine-5)-methyltransferase 1 (DNMT1) which would result in an apparent hypometylation. In order to assess the likelihood of

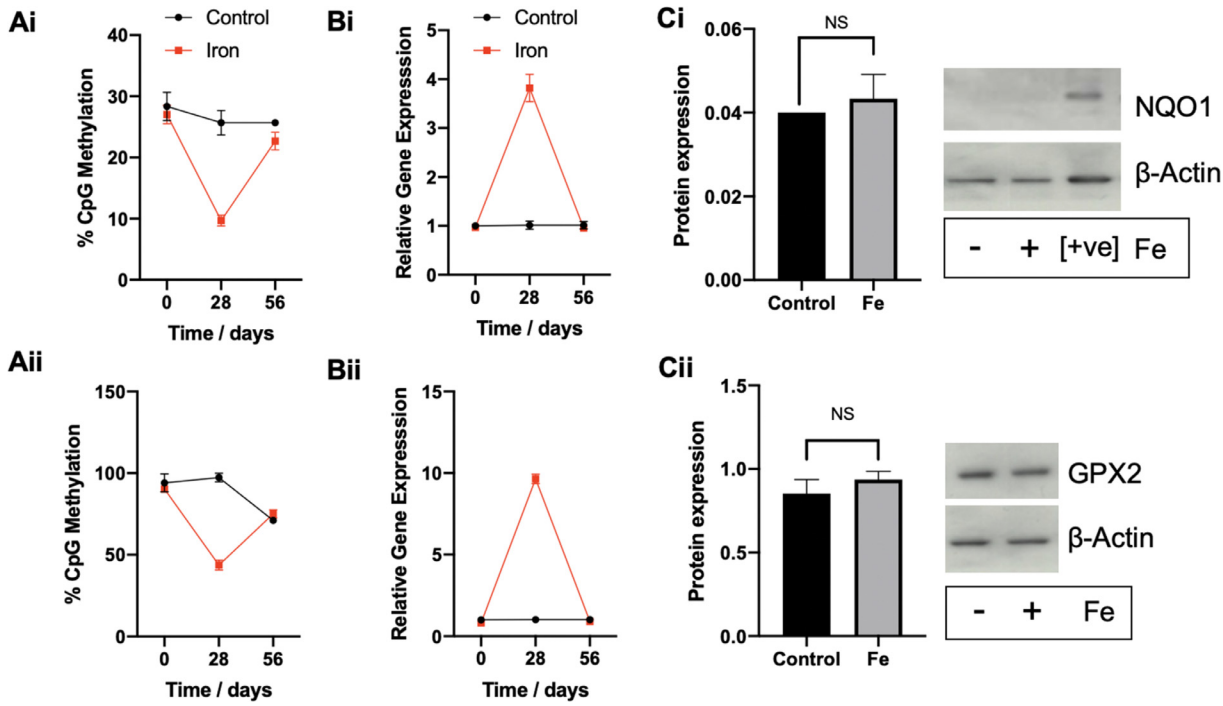

Fig. 5. Post co-culture decay of iron-induced epigenetic activation of NRF2 upon removal of iron. % Methylation changes in NQO1 and GPX2 (Ai and Aii respectively) at d 0, 28 (the period with iron co-culture) and at d 56 (the subsequent 28-d culture period with iron removed). Gene expression changes in NQO1 and GPX2 (Bi and Bii respectively) at d 0, 28 and 56. Protein expression changes in NQO1 and GPX2 (Ci and Cii respectively) at d 56. For NQO1, as very week bands are present in the control and iron treated groups at d-56, a recombinant NQO1 protein was utilised as a positive control. Data presented as mean values (n=3), with error bars representing +/- standard deviation. NRF2, nuclear factor erythroid 2-related factor 2.

transcription factor (TF) binding blockage of methylation, the genomic location and base-pair (BP) distance between the ARE and CG site under investigation was quantified (Fig. 7).

No correlation between degree of hypomethylation (% decrease) and distance from the ARE or NFE2 TFBS was identified for GPX2; comparatively high % degrees of hypomethylation were found close or in near to AREs or NFE2 TFBS relative to more distance CG sites of the gene. However, the GPX2, more distant CG sites from the ARE or NFE2 TFBS were found to be less demethylated, with relatively higher CG demethylation found near possible sites of DNMT1 blockade.

3.7. Demethylation status correlates with FTH1 expression in phenotypically iron-rich tissues

To identify if tissues that are iron-rich (as indicated by increased FTH1 expression) are increasingly demethylated at NQO1 and GPX2 CG sites, correlation analysis within normal colonic tissues was investigated (Fig. 8).

Significant negative correlations between NQO1 and GPX2 methylation status with FTH1 expression were found (R=-0.76 and -0.7 respectively). As FTH1 expression increases at elevated cellular iron concentrations, this correlation demonstrates that cells that are more iron-replete indeed have decreased CG methylation for NQO1 and GPX.

3.8. Hypomethylation changes evident in mice chronically administered iron

To further support if methylome changes are apparent in vivo, wild-type C57BL/6 mice were administered a diet either high or low in iron for a 28 d period. After this period, the intestinal mucosa were harvested and methylation analysis was undertaken on murine CG sites within neighbouring regions of the analogous human CG site identified on the methylation array (Fig. 9). There were no homologous CG sites present on the comparative murine genome for the GPX or NQO1 sites assessed, however, CG sites were identified within closely related (within +/- 100 bps) regions. Details on this can be found within the supporting information.

Not all CG sites sequenced were found to be significantly hypomethylated by iron. For NQO1, CG site 1 and 2 on Ms_06635059 were found to be 4.3 % (P=.007) and 5.0 % (P=.01) demethylated by iron (where the original hypomethylation effect on the analogous human site was 6.2 %). For GPX2, CG site 1 on Ms_19502457 was significantly demethylated by 13.4 % (P=.05) by iron (where the original hypomethylation extent on the analogous human site was 10.9 %). Additional sites demonstrated no changes in methylation and these differences did not correlate to CG location with respect to possible AREs that were identified or previously characterized NFE TFBS.

4. Discussion

The role of iron-excess in intestinal disease progression has been well documented. These iron-dependent processes are associated with various molecular pathways (for example oncogenic gene amplification, ROS-mediated cellular damage and intestinal microbiome alterations). In this study, we report the first finding of iron-dependent epigenetic changes that may describe a mechanism by which cells sense increasing oxidative stress due to dietary iron excess. Our experimental approach, where cells were chronically exposed (for 28 d) to iron, attempted to simulate a continued and prolonged exposure of enterocytes to iron which would occur in individuals consuming a high-iron diet [34]. Similarly, in the murine study mice were administered a high iron diet for a similar time period consuming on average 0.15 mg of iron per day. The

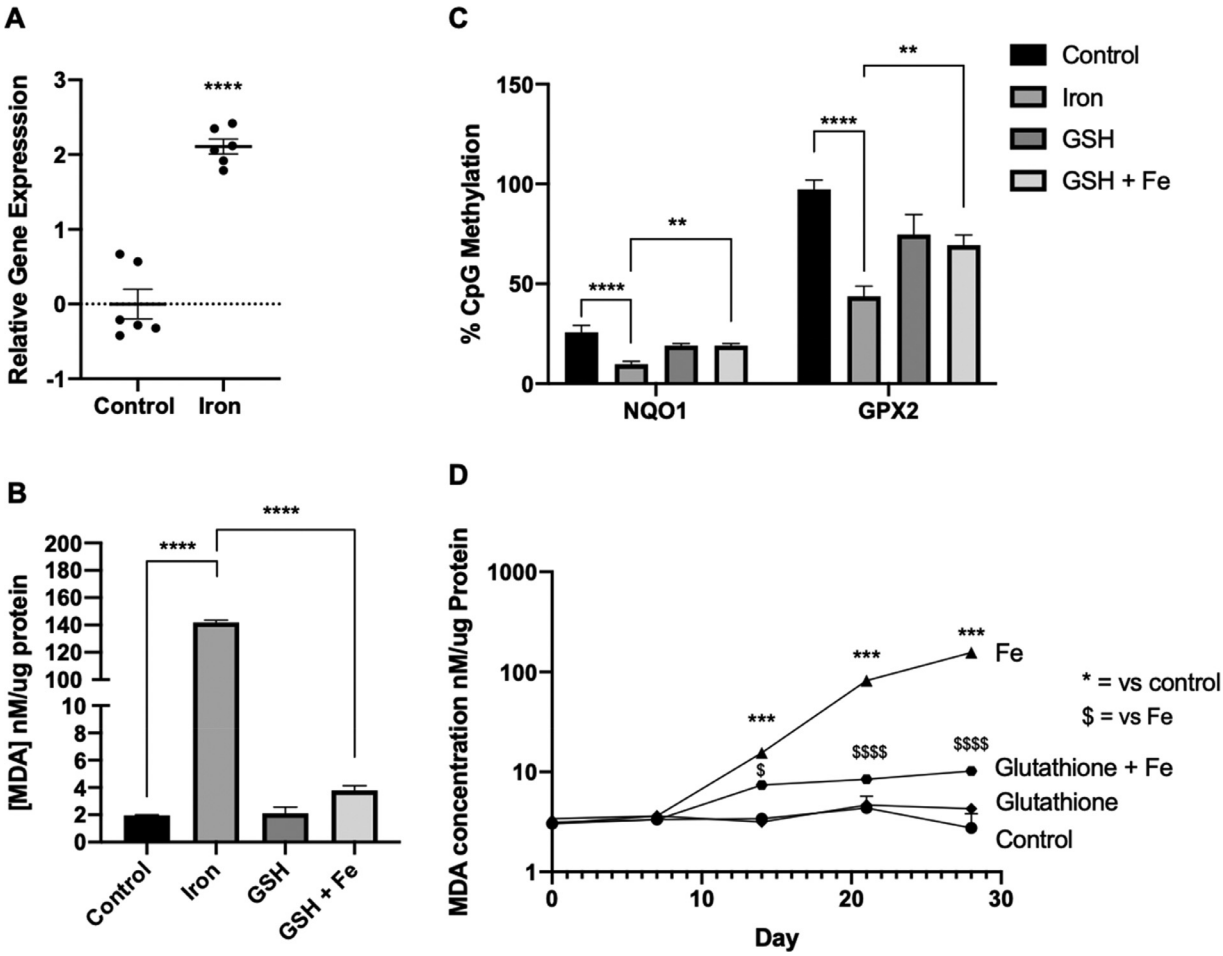

Fig. 6. Mechanistic insights into iron-dependent hypomethylation. (A) Caco-2 TET1 gene expression after 28-days of co-culture in the absence or presence of $FeSO_4$ (10 μM). (B) Caco-2 malondialdehyde [MDA] concentrations following 28-d co-culture with $FeSO_4$ (10 μM) +/- exogenous GSH (1 mM). (C) Caco-2 methylation changes at targeted CG sites within the genes of NOQ1 and GPX2 post co-cultured for 28-d with $FeSO_4$ (10 μM) +/- GSH (1 mM). (D) Time course Caco-2 MDA changes over a 28-d period of co-culture with $FeSO_4$ (10 μM) +/- exogenous GSH (1 mM). Data presented as mean values (n=3), with error bars representing +/- standard deviation. Significant changes examined using a paired students t-test or 2way ANOVA-multiple comparisons tests (where appropriate) where *, **, *** and **** denotes P<.05, .01, .001 and .0001 respectively.

concentration of iron within the colonic lumen is between 1.8–25 mM, present in individuals consuming regular Western diets [35–38]. These concentrations are observed due to the low absorption profile of iron in the proximal small intestine, where between 0.7 and 22.9 % of ingested non-heme iron is absorbed [39]. The concentration used in this study was indeed much less (10 μM) as cells in culture are non-viable at these higher, millimolar concentrations. After verifying that these culture conditions do alter cellular iron metabolism as expected, the impact of this regimen on DNA methylation was assessed. Remarkably, we report that iron co-culture induced hypomethylation changes only, with average $\delta\beta$ of 0.16 for all DMPs with β>10; no significant hypermethylation changes were found. We did not observe random, non-specific hypomethylation of CG sites within our studies but consistent and reproducible epigenetic changes were identified through pathway enrichment analyses.

Gene targets of the NRF2 pathway were found to be significantly enriched amongst the hypomethylated CG sites identified from the array (56 NRF2 targets with adj. P<.05); NQO1 and GPX2 were subsequently utilised for validation studies and indeed both were found to be significantly hypomethylated by iron. NQO1 and GPX2 hypomethylation led to increased gene expression and increased protein expression, confirming that iron is modulating NRF2 target gene expression via epigenetic modification. NQO1 and GPX2, a quinone reductase and glutathione peroxidase enzyme respectively are commonly upregulated in periods of cellular redox stress [40]. As such, since NRF2 targets are responsible for cellular detoxification and iron itself is a potent oxidant [41], hypomethylation of these targets could thus be in response to increased cellular oxidative stress. Canonical activation of NRF2 targets (through liberation of KEAP1) repression and subsequent antioxidant-responsive element gene expression) by iron-mediated oxidative stress is well established [42], yet no reports to date suggest the possibility of iron-dependent hypomethylation of NRF2 targets to induce expression in response to cellular oxidative stress as described here. We did find the NRF2 gene (NFE2L2) to be slightly demethylated (5.7 %) but this was not as significant as other NRF2 targets highlighted (beta value -0.81). Indeed, hypomethylation of NFE2L2 promotor CGs would indeed lead to expression of NRF2 targets, which has been documented for other bioactives [43].

Activation of NRF2 targets via iron-dependent hypomethylation may thus be an additional anti-oxidant defence mechanism, yet how iron orchestrates this hypomethylation is unknown. The finding that only hypomethylation changes were observed allude to the possible mechanistic nature of this effect. We have demonstrated that methylation status, subsequent gene and protein expression all return to basal levels when iron is removed and that chronic

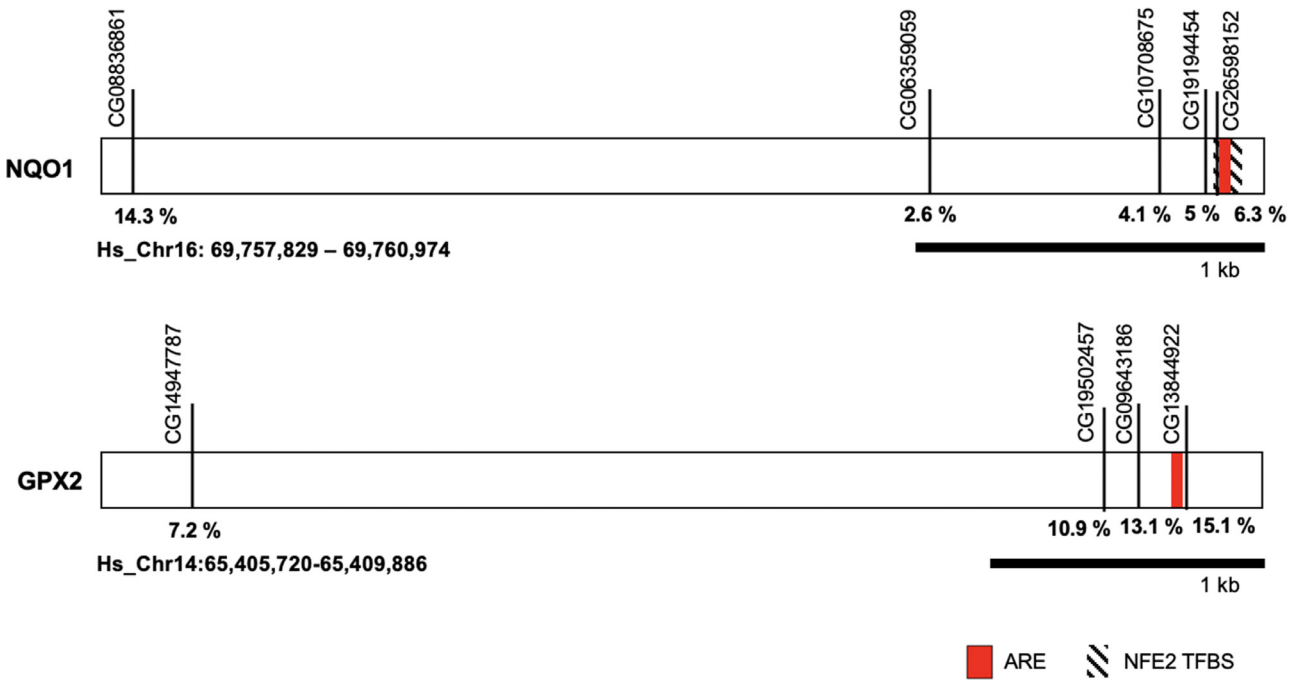

Fig. 7. Genomic mapping of CG, ARE and NFE2 TFB sites. (A) NQO1 and (B) GPX2 genomic location maps (to scale) for CG sites (denoted as black vertical lines) analyzed and their corresponding % hypomethylation of iron stated below. AREs are highlighted in red and NFE2 binding sites highlighted in black and white (where these have been previously characterized). ARE, antioxidant response elements.

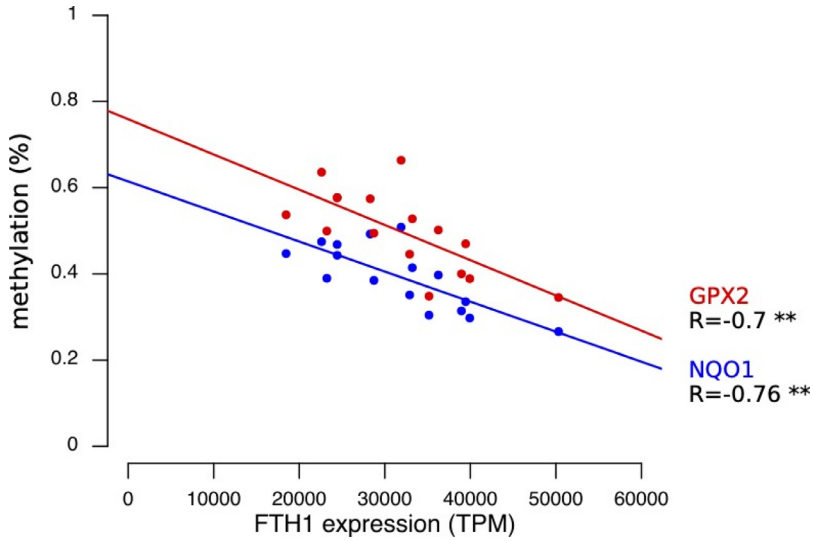

Fig. 8. Methylation status correlation with cellular iron status from TCGA data. (A) NQO1 and (B) GPX2 methylation status correlation with FTH1 expression. Data presented (n=16 total) for normal/healthy tissue with R values representing two-sided Pearson's product-moment correlation and ** denoting P<.005.

iron-exposure is required for significant hypomethylation changes to be observed. This implies that iron-dependent hypomethylation is not stimulated in an on/off manner (*i.e.,* through dynamic signaling initiated directly or indirectly by iron) but accumulation of the stimulus is needed. Similar time-dependent effects have also been observed in other studies examining the impact of dietary agents on epigenetic signatures, including curcumin and polyphenolic compounds [18]. In such studies, a sustained exposure is required as dietary agents have weak DNA modulating effects. However, longer-term models effectively mimic dietary-associated exposure and overtime influences so-called 'epigenetic memory'. This longer-term response thus lends itself to accumulation of cellular oxidation or oxidative-mediated cellular damage, where diminishment of cellular anti-oxidants results over the long period of iron exposure. In support of this, we monitored intracellular iron concentrations, the LIP, cellular lipid peroxidation, NQO1, and GPX2 gene, and protein expression and hypomethylation changes every 7 d over the 28 d iron co-culture period. The labile iron pool was significantly elevated with respect to the control cells only after 21 d of co-culture with iron. Similarly, this time dependence (21 d or longer) was observed for lipid peroxidation levels. NQO1 and GPX2 hypomethylation was also only found at d 21 onwards which similarly translated to NQO1 and GPX2 gene and protein expression changes after this time period. These data suggest that iron-

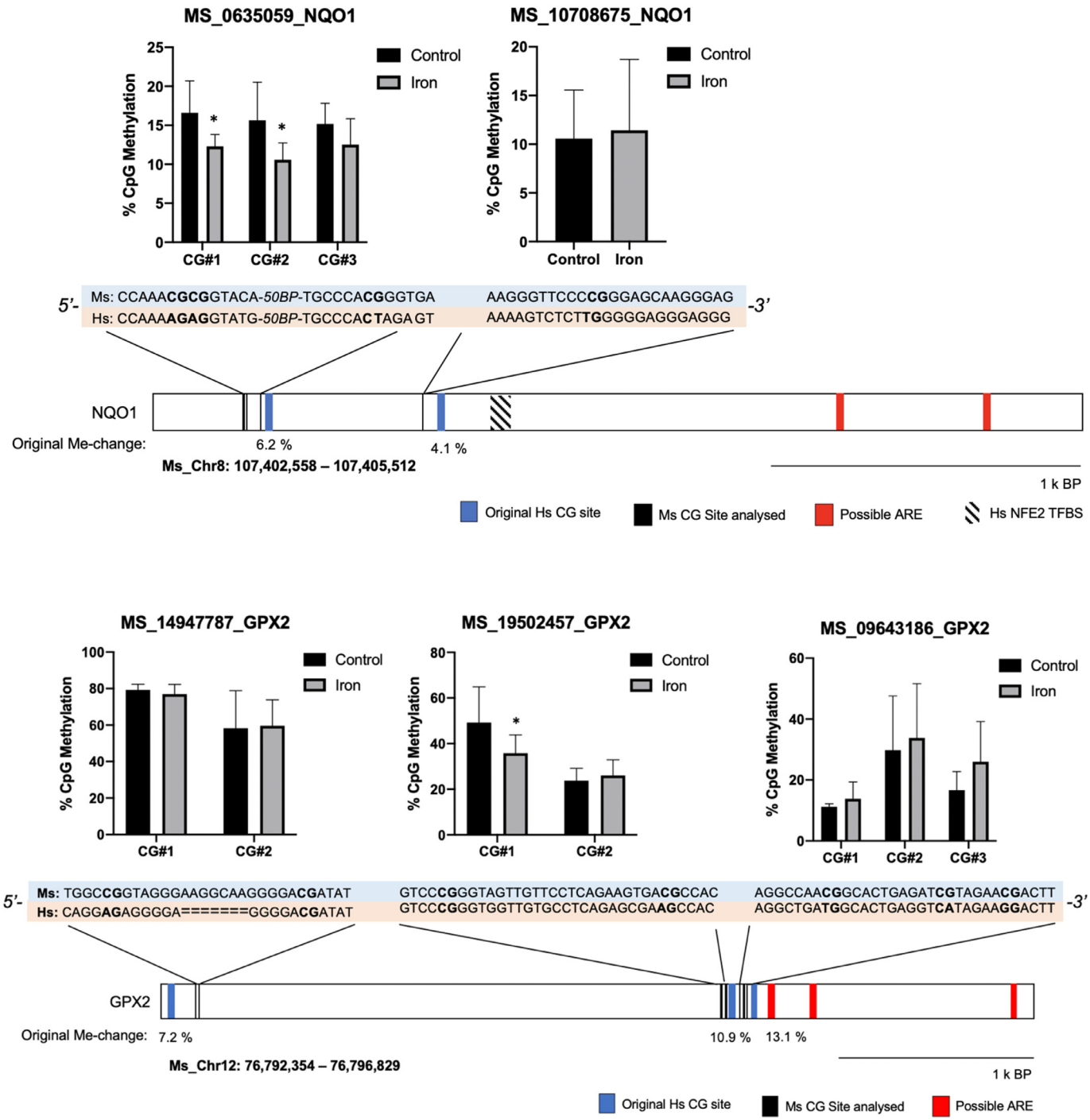

Fig. 9. Iron demethylates CG sites within the murine intestine. Methylation changes analyzed using pyrosequencing at targeted CG sites within the genes of (A) NQO1 and (B) GPX2 in murine intestinal mucosa from mice administered either a high (50 mg/kg) or low (3 mg/kg) ferrous sulphate supplemented diet. Data presented as mean values (n=8 in each group), with error bars representing +/- standard deviation. Significant changes examined using a paired students t-test where * P<.05. Below each chart, genomic location maps (to scale) for CG sites (denoted as black vertical lines) and their corresponding % hypomethylation (from the methylation array) are stated below. AREs are highlighted in red and NFE2 binding sites highlighted in black and white (where these have been previously characterised) and original human CG locations are highlighted in blue. Human and mouse DNA sequences for the CG sites analyzed have been expanded in full. ARE, antioxidant response elements.

loading is continually ongoing (as ferritin expression sequentially increased), yet, despite this, the LIP was elevated only after 21 d. At this point, the LIP is concentrated sufficiently to overcome intracellular anti-oxidant levels (since lipid peroxidation results after 21 d) and this (or indeed the high concentrations of intracellular ROS that are now likely to be present) drives the hypomethylation of NRF2 targets resulting in the observed gene and protein expression changes. The activation/induction of TET demethylating enzymes by electrophiles and ROS has been described elsewhere [44], and hence this is a reasonable postulate of how iron is inducing hypomethylation. TET enzymes coordinate the demethylation of DNA, and thus we monitored TET1 gene expression in Caco-2

treated cells with iron, and gene expression was elevated above the control. These results suggest that the iron-dependent hypomethylation we observed could be coordinated by TET1.

A 28 d co-culture with iron in the presence of exogenous GSH, acting as an antioxidant, was undertaken and this did not induce hypomethylation changes we observed for GPX2 and NQO1 with iron alone. It can be seen however that, even though GSH was acting as an antioxidant to reduce MDA concentrations, this was not complete (returning to baseline control) and this partial detoxification is mirrored with a non-complete return to % methylation levels in the GSH with Fe treated groups. From these results, the accumulation of iron and lipid peroxidation, or together as 'oxidative stress' could lead to the hypomethylation observed. This hypothesis is however speculative, as increased lipid peroxidation (MDA levels) does not directly correlate to increased ROS levels. Generating intracellular ROS independently of iron and then examining methylation changes would demonstrate the ROS-dependence of this phenomenon. Interestingly, many polyphenolic compounds that can modulate the epigenome additionally have iron-chelation activity, yet, their mechanism of action is likely through DNMT1 inhibition [45]. Whether iron chelators, independent of additional metabolic activities, could reverse iron-mediated hypomethylation needs to be examined. Furthermore, if iron chelation does dampen iron-mediated ROS production whilst also having an impact on epigenetic signatures, such details could confirm whether iron is orchestrating its effects independently of ROS. Indeed, the inhibitory effect of iron-chelation on TET1 activity has been reported [46]. This is because iron acts as a co-factor for TET1 and hence the inhibition of TET1 is correlated with iron-chelator binding potential [47]. On the other hand, ascorbic acid, another co-factor for TET1, also induces activity whilst having both anti-oxidant and iron-binding affinity [48].

To identify if the methylation changes described here are also found in human tissues, heathy colon tissue data from TCGA were extracted and examined. Evidently, being a cancer data repository, the majority of accessions are cancer-derived and only a small number (n=16) of healthy control colon samples were identified. Despite this small number, it was sufficient to see significant signals pertinent to this preliminary study. NQO1 and GPX2 correlation analysis with ferritin expression was undertaken and significant negative relationships were found. Ferritin expression was utilized here as a surrogate marker for tissue iron status (and hence high levels of ferritin indicate higher cellular iron concentrations). When NQO1 and GPX2 methylation status is correlated with FTH1 expression in healthy tissues, a significant negative association is found, implying that cells with higher iron levels do indeed demonstrate higher rates of NQO1 and GPX hypomethylation. This demonstrates that high iron-status *in vivo* is associated with NRF2-target hypomethylation.

Ferritin expression is also a target via canonical NRF2 activation, thus iron treatment is likely to be inducing ferritin expression through this route. However, as some FTH1 hypomethylation was observed (CG09367425: β=5.4, 11.9 % hypomethylation; CG24496614: β=3.9, 6.2% hypomethylation; CG01209023: β=0.51, 5.0% hypomethylation), iron-directed hypomethylation, as with the targets discussed above, could also be contributing towards protein expression. Uncoupling canonical *vs*. epigenetic driven activation of NRF2 targets by iron will provide important future mechanistic insights. Further to this, canonical binding of NRF2 to AREs could block DNMT1 access and methylation of neighboring CG sites. This has indeed been documented for other transcription factors [49], and would result in decreased methylation (and not hypomethylation, as described here). We sought to examine the likelihood of this by identifying if there is a correlation between the degree of hypomethylation found and CG distance from AREs or known NRF2 transcription factor binding sites; no significant correlations was found. However, it is still unknown how transcription factor binding could act as a blockade for DNMT1 access and hence methylation, particularly for NRF2. Interestingly, some CG sites actually dissect NRF2 AREs and hence, it would be expected that these would be significantly non-methylated if DNMT1 was being blocked by NRF2 binding.

The demethylating effect of iron was further validated in vivo utilizing a murine model administered a high iron diet. Homologous CG sites in the murine genome to the human CG sites analyzed throughout this study were not present, however, neighboring CG sites were identified and methylation status was analyzed. Some CG sites on both GPX2 and NQO1 genes did demonstrate significant hypomethylation in the iron-fed mice compared to controls, yet others did not. This could be because these murine CG homologs were non-identical, or, had little influence on target expression. This further highlights the need to understand the influence of CG methylation status and the subsequent impact on gene expression; these non-demethylated CG sites might not influence target gene expression like the CG sites identified and examined in this study. Additionally, studies have demonstrated that dietary-associated epigenetic alterations can be both cell and genotype-specific; therefore, the sites that iron is directing hypomethylation are specific [18]. In a similar analysis in the corresponding human gene sequences, the extent of hypomethylation could not be explained by location or distance from potential AREs or in terms of distance from the original CG loci. The variability in methylation status could also be attributed to the cellular heterogeneity of the cell populations in the mucosa. Despite this, several sites were significantly demethylated and the influence of these CG sites on gene expression needs to be quantified. Intestinal murine NQO1 and GPX2 expression was also quantified. The fold change in the Fe treated group for NQO1 and GPX was 1.8 and 1.3 respectively; this however was non-significant (data not shown). This again reaffirms the need to recognize the consequences of CG site methylation on gene expression, particularly if gene expression is controlled via epigenetic methods.

In conclusion, this is the first report to demonstrate that iron activates NRF2 targets via the epigenome. The most likely candidate for orchestrating these events is ROS via TET enzymes, but further validation of this mechanism is required. In addition, deconvolution of this iron-mediated hypomethylation mechanism from canonical activation of NRF2 should be undertaken. The finding that demethylating effects occur *in vivo* demonstrate the likelihood of NRF2 target activation via epigenetic alteration in individuals consuming a high iron diet or taking iron supplements, and could be a route by which cells overcome persistent and chronic oxidative stress. Consequently, such effects could have important implications iron-driven diseases, in particular cancer, where sustained oxidative stress is maintained to drive oncogenic transformation whilst evading ferroptosis and cell death.

Acknowledgments

The results described here are in whole or part based upon data generated by the TCGA Research Network: https://www.cancer.gov/tcga.

Declaration of Competing Interests

All authors declare no conflicts of interest.

Funding

GVG and AA acknowledges from support the NIHR Birmingham ECMC, NIHR Birmingham SRMRC, Nanocommons H2020-EU

(731032) and the NIHR Birmingham Biomedical Research Centre and the MRC Heath Data Research UK (HDRUK/CFC/01), an initiative funded by UK Research and Innovation, Department of Health and Social Care (England) and the devolved administrations, and leading medical research charities.

The views expressed in this publication are those of the authors and not necessarily those of the NHS, the National Institute for Health Research, the Medical Research Council or the Department of Health.

References

[1] LihBrody L, Powell SR, Collier KP, Reddy GM, Cerchia R, Kahn E, et al. Increased oxidative stress and decreased antioxidant defenses in mucosa of inflammatory bowel disease. Dig Dis Sci 1996;41(10):2078–86.
[2] Aghdassi E, Carrier J, Cullen J, Tischler M, Allard JP. Effect of iron supplementation on oxidative stress and intestinal inflammation in rats with acute colitis. Dig Dis Sci 2001;46(5):1088–94.
[3] Seril DN, Liao J, Yang GY, Yang CS. Oxidative stress and ulcerative colitis-associated carcinogenesis: studies in humans and animal models. Carcinogenesis 2003;24(3):353–62.
[4] Brookes MJ, Boult J, Roberts K, Cooper BT, Hotchin NA, Matthews G, et al. A role for iron in Wnt signalling. Oncogene 2008;27(7):966–75.
[5] Brookes MJ, Hughes S, Turner FE, Reynolds G, Sharma N, Ismail T, et al. Modulation of iron transport proteins in human colorectal carcinogenesis. Gut 2006;55(10):1449–60.
[6] Radulescu S, Brookes MJ, Salgueiro P, Ridgway RA, McGhee E, Anderson K, et al. Luminal iron levels govern intestinal tumorigenesis after Apc Loss In Vivo. Cell Rep 2012;2(2):270–82.
[7] Chua ACG, Klopcic BRS, Ho DS, Fu K, Forrest CH, Croft KD. Dietary iron enhances colonic inflammation and IL-6/IL-11-Stat3 signaling promoting colonic tumor development in mice. PLoS One 2013;8(11):12.
[8] Constante M, Fragoso G, Lupien-Meilleur J, Calve A, Santos MM. Iron supplements modulate colon microbiota composition and potentiate the protective effects of probiotics in dextran sodium sulfate-induced colitis. Inflamm Bowel Dis 2017;23(5):753–66.
[9] Werner T, Wagner SJ, Martinez I, Walter J, Chang JS, Clavel T. Depletion of luminal iron alters the gut microbiota and prevents Crohn's disease-like ileitis. Gut 2011;60(3):325–33.
[10] Statovci D, Aguilera M, MacSharry J, Melgar S. The impact of western diet and nutrients on the microbiota and immune response at mucosal interfaces. Front Immunol 2017;8:838.
[11] Seril DN, Liao J, Ho K-LK, Warsi A, Yang CS, Yang G-Y. Dietary iron supplementation enhances DSS-induced colitis and associated colorectal carcinoma development in mice. Dig Dis Sci 2002;47(6):1266–78.
[12] Gasche C, Lomer MCE, Cavill I, Weiss G. Iron, anaemia, and inflammatory bowel diseases. Gut 2004;53(8):1190–7.
[13] Chieppa M, Galleggiante V, Serino G, Massaro M, Santino A. Iron chelators dictate immune cells inflammatory ability: potential adjuvant therapy for IBD. Curr Pharm Des 2017;23(16):2289–98.
[14] Bastide NM, Pierre FH, Corpet DE. Heme iron from meat and risk of colorectal cancer: a meta-analysis and a review of the mechanisms involved. Cancer Prev Res 2011;4(2):177–84.
[15] GRØNBÆK K, Hother C, Jones PA. Epigenetic changes in cancer. Apmis 2007;115(10):1039–59.
[16] Davis CD, Uthus EO. Dietary selenite and azadeoxycytidine treatments affect dimethylhydrazine-induced aberrant crypt formation in rat colon and DNA methylation in HT-29 cells. J Nutr 2002;132(2):292–7.
[17] Link A, Balaguer F, Goel A. Cancer chemoprevention by dietary polyphenols: promising role for epigenetics. Biochem Pharmacol 2010;80(12):1771–92.
[18] Link A, Balaguer F, Shen Y, Lozano JJ, Leung H-CE, Boland CR, et al. Curcumin modulates DNA methylation in colorectal cancer cells. PLoS One 2013;8(2) e57709-e57709.
[19] Morris TJ, Butcher LM, Feber A, Teschendorff AE, Chakravarthy AR, Wojdacz TK, et al. ChAMP: 450k chip analysis methylation pipeline. Bioinformatics 2014;30(3):428–30.
[20] Chong J, Wishart DS, Xia J. Using metaboanalyst 4.0 for comprehensive and integrative metabolomics data analysis. Curr Protoc Bioinformatics 2019;68(1):e86.
[21] Kent WJ, Sugnet CW, Furey TS, Roskin KM, Pringle TH, Zahler AM, et al. The human genome browser at UCSC. Genome Res 2002;12(6):996–1006.
[22] Banning A, Deubel S, Kluth D, Zhou Z, Brigelius-Flohé R. The GI-GPx Gene Is a Target for Nrf2. Mole Cell Biol 2005;25(12):4914–23.
[23] Raghunath A, Sundarraj K, Nagarajan R, Arfuso F, Bian J, Kumar AP, et al. Antioxidant response elements: Discovery, classes, regulation and potential applications. Redox Biol 2018;17:297–314.
[24] Namani A, Liu K, Wang S, Zhou X, Liao Y, Wang H, et al. Genome-wide global identification of NRF2 binding sites in A549 non-small cell lung cancer cells by ChIP-Seq reveals NRF2 regulation of genes involved in focal adhesion pathways. Aging (Albany NY) 2019;11(24):12600.
[25] Jain A, Lamark T, Sjøttem E, Larsen KB, Awuh JA, Øvervatn A, et al. p62/SQSTM1 is a target gene for transcription factor NRF2 and creates a positive feedback loop by inducing antioxidant response element-driven gene transcription. J Biol Chem 2010;285(29):22576–91.
[26] Horniblow RD, Bedford M, Hollingworth R, Evans S, Sutton E, Lal N, et al. BRAF mutations are associated with increased iron regulatory protein-2 expression in colorectal tumorigenesis. Cancer Sci 2017;108(6):1135–43.
[27] Rebouche CJ, Wilcox CL, Widness JA. Microanalysis of non-heme iron in animal tissues. J Biochem Biophys Methods 2004;58(3):239–51.
[28] Network CGA. Comprehensive molecular characterization of human colon and rectal cancer. Nature 2012;487(7407):330.
[29] Grossman RL, Heath AP, Ferretti V, Varmus HE, Lowy DR, Kibbe WA, et al. Toward a shared vision for cancer genomic data. N Engl J Med 2016;375(12):1109–12.
[30] Colaprico A, Silva TC, Olsen C, Garofano L, Cava C, Garolini D, et al. TCGAbiolinks: an R/Bioconductor package for integrative analysis of TCGA data. Nucleic Acids Res 2016;44(8) e71-e71.
[31] Mounir M, Lucchetta M, Silva TC, Olsen C, Bontempi G, Chen X, et al. New functionalities in the TCGAbiolinks package for the study and integration of cancer data from GDC and GTEx. PLoS Comput Biol 2019;15(3):e1006701.
[32] Silva TC, Colaprico A, Olsen C, D'Angelo F, Bontempi G, Ceccarelli M, et al. TCGA Workflow: Analyze cancer genomics and epigenomics data using Bioconductor packages. F1000Research 2016:5.
[33] Slenter DN, Kutmon M, Hanspers K, Riutta A, Windsor J, Nunes N, et al. WikiPathways: a multifaceted pathway database bridging metabolomics to other omics research. Nucleic Acids Res 2018;46(D1):D661–7.
[34] Collings R, Harvey LJ, Hooper L, Hurst R, Brown TJ, Ansett J, et al. The absorption of iron from whole diets: a systematic review. Am J Clin Nutr 2013;98(1):65–81.
[35] Lund, E.K.; Wharf, S.G.; Fairweather-Tait, S.J.; Johnson, I.T.J.T.A. j. o. c. n., Oral ferrous sulfate supplements increase the free radical–generating capacity of feces from healthy volunteers. 1999, 69 (2), 250-255.
[36] Pizarro, F.; Amar, M.; Stekel, A.J.T.A.j.o.c.n., Determination of iron in stools as a method to monitor consumption of iron-fortified products in infants. 1987, 45 (2), 484-487.
[37] Yilmaz B, Li H. Gut Microbiota and Iron: The Crucial Actors in Health and Disease. Pharmaceuticals (Basel) 2018;11(4):98.
[38] Lund EK, Wharf SG, Fairweather-Tait SJ, Johnson IT. Increases in the concentrations of available iron in response to dietary iron supplementation are associated with changes in crypt cell proliferation in rat large intestine. J Nutr 1998;128(2):175–9.
[39] Collings R, Harvey LJ, Hooper L, Hurst R, Brown TJ, Ansett J, et al. The absorption of iron from whole diets: a systematic review. Am J Clin Nutr 2013;98(1):65–81.
[40] Ross D, Siegel D. NQO1 in protection against oxidative stress. Curr Opin Toxicol 2018;7:67–72. https://www.sciencedirect.com/science/article/pii/S2468202017301237.
[41] Lee J-M, Calkins MJ, Chan K, Kan YW, Johnson JA. Identification of the NF-E2-related factor-2-dependent genes conferring protection against oxidative stress in primary cortical astrocytes using oligonucleotide microarray analysis. J Biol Chem 2003;278(14):12029–38.
[42] Kaspar JW, Niture SK, Jaiswal AK. Nrf2: INrf2 (Keap1) signaling in oxidative stress. Free Radic. Biol Med 2009;47(9):1304–9.
[43] Khor TO, Huang Y, Wu T-Y, Shu L, Lee J, Kong A-NT. Pharmacodynamics of curcumin as DNA hypomethylation agent in restoring the expression of Nrf2 via promoter CpGs demethylation. Biochem Pharmacol 2011;82(9):1073–8.
[44] Kang K, Piao M, Kim K, Kang H, Chang W, Park I, et al. Epigenetic modification of Nrf2 in 5-fluorouracil-resistant colon cancer cells: involvement of TET-dependent DNA demethylation. Cell Death Dis 2014;5(4) e1183-e1183.
[45] Fang M, Chen D, Yang CS. Dietary polyphenols may affect DNA methylation. J Nutr 2007;137(1) 223S–228S.
[46] Jakubek M, Kejík Z, Kaplánek R, Antonyová V, Hromádka R, Šandriková V, et al. Hydrazones as novel epigenetic modulators: Correlation between TET 1 protein inhibition activity and their iron (II) binding ability. Bioorg Chem 2019;88:102809.
[47] Rasmussen KD, Helin K. Role of TET enzymes in DNA methylation, development, and cancer. Genes Develop 2016;30(7):733–50.
[48] Blaschke K, Ebata KT, Karimi MM, Zepeda-Martínez JA, Goyal P, Mahapatra S, et al. Vitamin C induces Tet-dependent DNA demethylation and a blastocyst–like state in ES cells. Nature 2013;500(7461):222–6.
[49] Domcke S, Bardet AF, Ginno PA, Hartl D, Burger L, Schübeler D. Competition between DNA methylation and transcription factors determines binding of NRF1. Nature 2015;528(7583):575–9.